

On the determination of cyclic strain history

Th. Triantafyllidis, T. Wichtmann & A. Niemunis

Institute of Soil Mechanics and Foundation Engineering, Ruhr-University Bochum

ABSTRACT: The information about the void ratio and the stress is not sufficient to predict the deformation accumulation rate under cyclic loading of definite amplitude. The rate of accumulation is significantly affected by cyclic preloading. For an accurate prediction of the accumulation the determination of cyclic preloading history is of high importance. In this paper we search for appropriate methods to determine the preloading history *in situ*. It is demonstrated, that a cyclic preloading cannot be correlated with small strain stiffness. A correlation with material damping or the undrained cyclic material behaviour is somewhat more promising. An alternative approach for shallow layers using heavy vibration is proposed.

1 INTRODUCTION

The importance of cyclic preloading history concerning the accumulation rate is illustrated in Figure 1. The reduction of void ratio e in three cyclic triaxial tests with identical average and cyclic loads but slightly different initial void ratios e_0 is presented. Considering a state of identical void ratio (marked by the solid horizontal line) the accumulation rate $\dot{e} = \partial e / \partial N$ of the freshly pluviated specimen is higher in comparison with the rates of those specimens, that had already been subject to several thousands of load cycles. Thus, at the same average stress, amplitude of cyclic loading and void ratio cyclic preloading significantly affects the cumulative behaviour of a soil.

Niemunis et al. (2004) and Wichtmann et al. (2004a,b) present an explicit constitutive model for sand under cyclic loading and its experimental evidence. The formulas were derived from laboratory tests performed on freshly pluviated specimens. However, an accumulation under cyclic loading *in situ* is slower due to a cyclic preloading history from seismic activity, sedimentation and erosion processes (in the case of natural deposits), construction site machines or mechanical densification processes (especially in the case of artificial deposits). Thus, using the constitutive model and starting the calculation with $N = 0$ (corresponds to the freshly pluviated laboratory specimen without any cyclic preloading) could strongly overestimate the accumulation of deformation or the pore water pressure development. Therefore, it is of crucial importance to determine the cyclic preloading history of a soil and to introduce it into the calcula-

tion.

This paper presents our search for methods to determine the cyclic preloading history. A correlation of cyclic preloading history with the small strain stiffness (dynamic soil property, measurable *in situ* cross hole or down hole) was tested. The theoretical basis for such correlation is given. Unfortunately, no experimental validation of the hypothesis could be obtained from the results of resonant column tests and from cyclic triaxial tests with measurement of small strain compression and shear wave velocities. It was found that the small strain stiffness is sparsely affected by cyclic preloading.

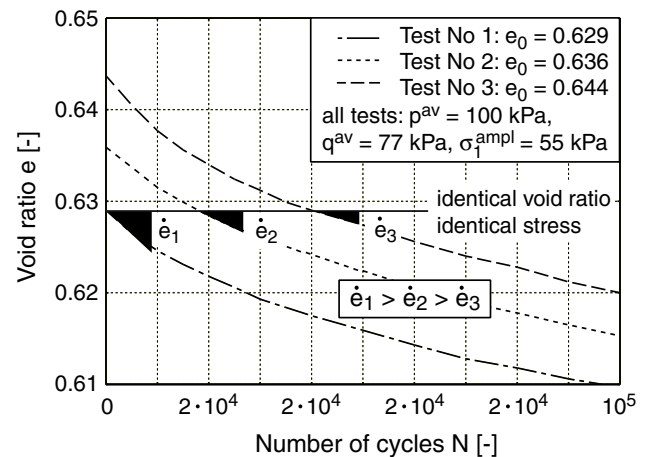


Figure 1. Influence of a cyclic preloading history on the accumulation rate \dot{e} in drained cyclic triaxial tests

A correlation of cyclic preloading with material damping is outlined. Furthermore, it is demonstrated, that cyclic preloading significantly affects the cyclic

undrained material behaviour and thus, for saturated soils the cyclic preloading history could possibly be determined *in situ* via measurements of pore water pressure development in cone penetration tests.

For shallow soil layers it is proposed to measure the settlement and settlement accumulation of a heavy vibrator on the surface after a number of excitation cycles. The cyclic preloading history could be calculated back from the measured curve of the settlement over time.

2 CORRELATION OF CYCLIC STRAIN HISTORY WITH DYNAMIC SOIL PROPERTIES

2.1 Motivation

Cyclic loading changes the fabric of an assemblage of grains, i.e. the number of particle contacts, their orientation and shape are varied. With increasing number of cycles the soil fabric becomes more resistant against further accumulation. This is due to an increase of the coordination number (number of contacts per grain), smaller spatial fluctuation of grain-to-grain forces etc.

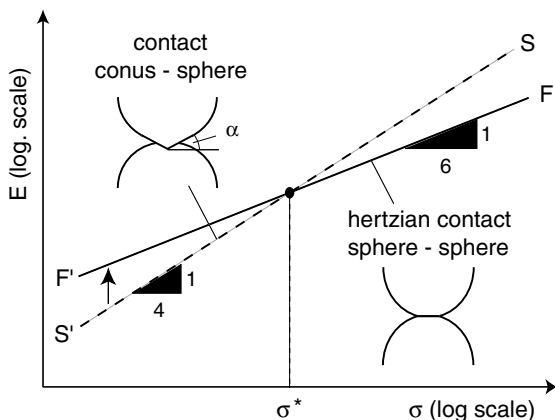


Figure 2. Comparison of stiffness of contact types "sphere-sphere" and "conus-sphere"

The stiffness E and the elastic energy W of an elastic contact of two ideal spheres with an equal radius R loaded by an axial force F was derived by Hertz (1881):

$$E = \frac{3}{2} \left[\frac{2\bar{G}}{3(1-\bar{\nu})} \right]^{\frac{2}{3}} \sigma^{\frac{1}{3}} \quad (1)$$

$$W = \frac{4^{\frac{8}{3}}}{5} \left[\frac{3(1-\bar{\nu})}{8\bar{G}} \right]^{\frac{2}{3}} R^{\frac{4}{3}} \sigma^{\frac{5}{3}} \quad (2)$$

with \bar{G} and $\bar{\nu}$ being the shear modulus and the Poisson's ratio of the sphere material. For a simple cube packing $\sigma = F/D^2$ is the stress in the axial direction. Goddard (1990) derived the corresponding modulus

and energy of a contact of a conus (asperity α) and a sphere:

$$E = \left(\frac{\bar{G}}{1-\bar{\nu}} \right)^{\frac{1}{2}} \left(\frac{6}{\pi\alpha} \right)^{\frac{1}{2}} \sigma^{\frac{1}{2}} \quad (3)$$

$$W = \frac{4^{\frac{3}{2}}}{3} \left[\frac{3(1-\bar{\nu})}{8\bar{G}} \right]^{\frac{1}{2}} (\pi\alpha)^{\frac{1}{2}} R^3 \sigma^{\frac{3}{2}} \quad (4)$$

Goddard assumed Equation (3) to be valid in the case of pressures σ below a transition pressure σ^* which can be deduced from Equations (1) and (3):

$$\sigma^* = \frac{1}{96} \frac{\bar{G}}{1-\bar{\nu}} \pi^3 \alpha^3 \quad (5)$$

For $\sigma > \sigma^*$ Equation (1) is valid. This is shown schematically in Figure 2. The curve F'-F is calculated from Equation (1) and S'-S corresponds to Equation (3). Goddard thought of Figure 2 as a kind of "thermodynamic" phase diagram with the more stable phase being represented by the curve F'-F (contact sphere - sphere) and with S'-S (contact conus - sphere) being a metastable phase. The transition pressure σ^* is strongly dependent on the asperity α , see Figure 2. Goddard assumed that during vibration the relatively soft contacts of the type "conus - sphere" are replaced by stiffer and more stable Hertzian contacts due to particle re-orientation and abrasion effects. The possible increase of stiffness due to a transition of the shape of a particle contact is indicated by the vertical arrow in Figure 2.

Changes of stiffness and energy of an assemblage of ideal spheres caused by an abatement of spatial stress fluctuation are demonstrated by the simple example presented in Figure 3. In case (a) the whole external force $2F$ is carried by one column and in case (b) it is distributed evenly. Assuming a Hertzian contact law the relations $E_b/E_a = 2^{\frac{2}{3}}$ (E_{\square} : stiffness for case \square corresponding to Fig. 3) and $W_b/W_a = 2^{-\frac{2}{3}}$ are valid. Since a particle assemblage should spontaneously tend towards the state of the lowest possible energy it is expected that vibration of dry particles leads to a reduction of stress fluctuation and thus, to a higher stiffness.

A more elaborate study concerning energies resulting from different stress fluctuations in particle assemblages using the "q-model" of Coppersmith (1996) is documented by Triantafyllidis & Niemunis (2000).

These theoretical considerations were supported by test results of Drnevich & Richart (1970) who found the small strain shear modulus G_0 to increase strongly under a repeated torsional shearing in the resonant column device (Fig. 4). However, the literature is not

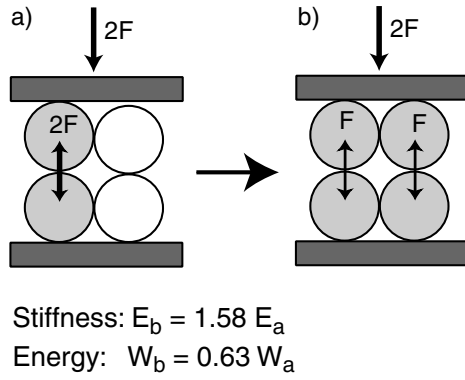


Figure 3. Reduction of stress fluctuation as a cause of stiffness increase and energy decrease

unanimous concerning the influence of cyclic strains on small strain stiffness. While some authors (e.g. Drnevich & Richart 1970, Shen et al. 1985) found a stiffness increase some others did not (e.g. Alarcon-Guzman et al. 1989, Lo Presti et al. 1993, Teachavorasinskun et al. 1994). A more detailed review is given by Wichtmann & Triantafyllidis (2004a,b).

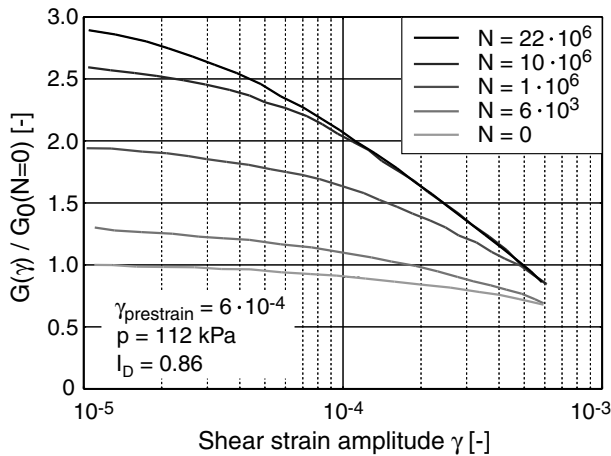


Figure 4. Increase of small strain stiffness G_0 due to torsional prestraining in Resonant Column tests after Drnevich and Richart (1970)

2.2 Resonant Column (RC) Tests

The effect of a prestraining history on shear modulus and material damping was studied in resonant column tests. Details of the device and the specimen preparation method (dry pluviation through air) were given by Wichtmann et al. (2001). Some test data concerning the dependence of the dynamic properties of the sands under consideration on stress, void ratio and time can be found in Wichtmann & Triantafyllidis (2004a,b).

One fine and two medium grained sands were used in this test series documented in this paper. The grain distribution curves are given in Figure 5 while the minimum and maximum densities as well as some characteristic quantities of the grain distri-

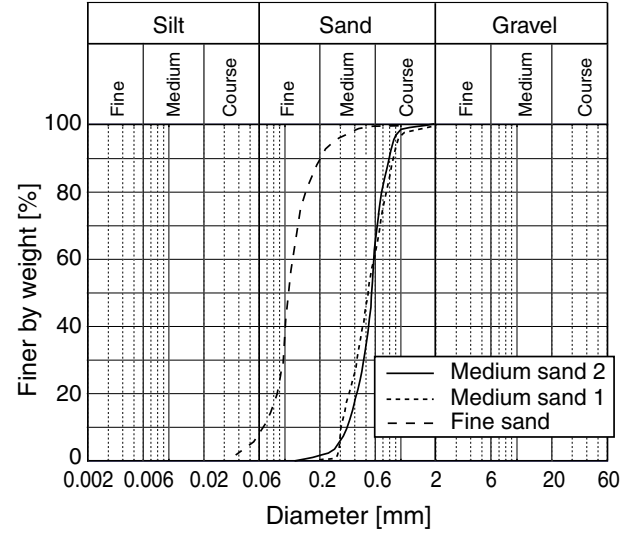


Figure 5. Grain distribution curves of tested materials

Sand	ρ_s	$\rho_{d,min}$	$\rho_{d,max}$	d_{50}	U
	[g/cm ³]	[g/cm ³]	[g/cm ³]	[mm]	[-]
Fine sand	2.65	1.453	1.753	0.11	1.7
Medium sand 1	2.65	1.437	1.715	0.51	2.0
Medium sand 2	2.65	1.414	1.680	0.55	1.8

Table 1. Minimum / maximum densities and grain size characteristics of used sands

bution curves (mean diameter d_{50} , uniformity index $U = d_{60}/d_{10}$) are summarized in Table 1.

In a first test series a dynamic torsional prestraining was applied to full (not hollow) cylindrical specimens in the RC device. The tests were conducted on the fine sand and the medium sand 1 with a medium density ($0.62 \leq I_{D0} \leq 0.68$). Two different prestraining amplitudes ($\gamma_{prestrain} = 5 \cdot 10^{-5}$ and $\gamma_{prestrain} = 1 \cdot 10^{-4}$) and different maximum numbers of cycles N_{max} were studied.

After the application of the confining pressure the shear strain amplitude γ was increased up to $\gamma_{prestrain}$ and a definite number of cycles was applied. Next the shear strain amplitude was reduced to the lowest possible value in order to measure the shear modulus at small strains $G_0 = G(\gamma \approx 10^{-6})$. Having reached the desired maximum number of cycles N_{max} the curves $G(\gamma)$ and $D(\gamma)$ were measured over the whole range of applicable shear strains in order to observe changes of the shape of these curves due to cyclic torsional loading.

Figure 6 presents typical curves of shear modulus and damping ratio versus shear strain amplitude. After the first package of cycles a slight reduction of G_0 in comparison with the value of a non-prestrained specimen was observed. During the subsequent torsional prestraining only a slight increase of G_0 could be detected (see also Fig. 7). At $N = N_{max}$ the curves

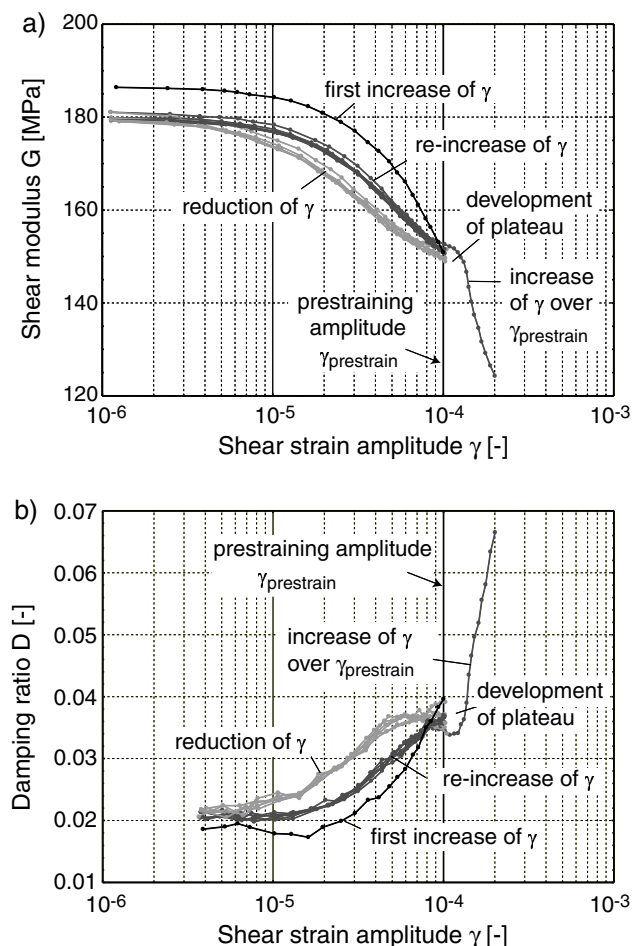


Figure 6. Development of plateaus in the curves a) $G(\gamma)$ and b) $D(\gamma)$ due to dynamic prestraining in the RC device, test on dry fine sand with $N_{\max} = 3 \cdot 10^6$ cycles, confining pressure $p = 200$ kPa and initial relative density $I_{D,0} = 0.64$

$G(\gamma)$ and $D(\gamma)$ exhibited a plateau around the prestraining amplitude $\gamma_{\text{prestrain}}$. These plateaus were already reported by Li et al. (1998a,b, 1999). They become more pronounced with increasing prestraining, i.e. with the number of cycles and the prestraining amplitude (Wichtmann & Triantafyllidis 2004a). Evidently, sand memorizes not only the prestraining amplitude but also the number of applied cycles. If packages of cycles with different amplitudes $\gamma_{\text{prestrain}}$ were applied, the sequence of these packages was of importance for the shape of the resulting curves $G(\gamma)$ and $D(\gamma)$ (Wichtmann & Triantafyllidis 2004a). A change of stress after prestraining blurred the signature of cyclic strain history (Wichtmann & Triantafyllidis 2004a). No significant differences in the material behaviour could be detected, if hollowed cylindrical specimens (shear strains more evenly distributed over the cross section) were used (Wichtmann & Triantafyllidis 2004a).

The strain amplitudes during torsional prestraining in the resonant column device were relatively small. In an additional test series hollow cylinder specimens were cyclically (0.5 Hz) prestrained at $\gamma_{\text{prestrain}} \geq 5 \cdot 10^{-3}$ in a special torsional shear device. They had dif-

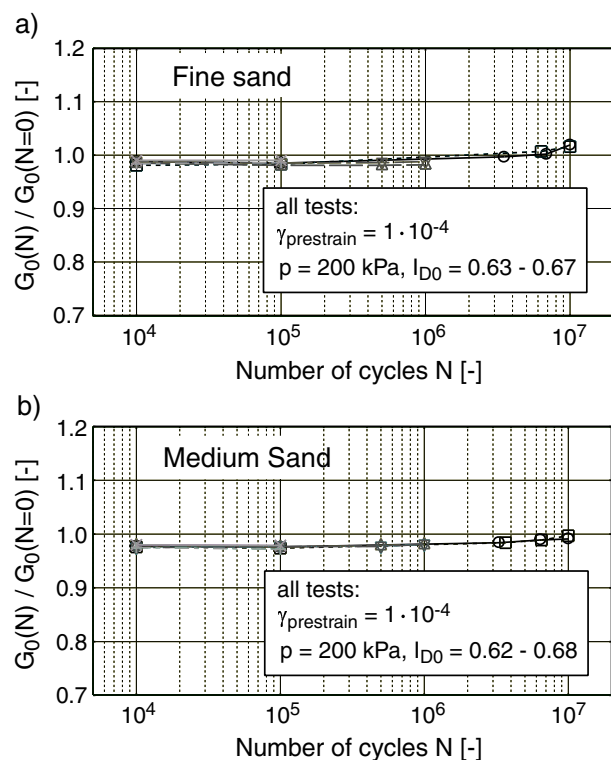


Figure 7. Evaluation of G_0 with the number of cycles during dynamic torsional prestraining with $\gamma_{\text{prestrain}} = 10^{-4}$ in the RC device, tests with different maximum numbers of cycles N_{\max}

ferent initial densities and the number of prestraining cycles was varied. After prestraining the specimens were placed into the RC device in order to measure the small strain stiffness G_0 as well as the curves $G(\gamma)$ and $D(\gamma)$. Figure 8 presents the shear moduli of specimens prestrained with $\gamma_{\text{prestrain}} = 5 \cdot 10^{-3}$ versus the void ratio e after prestraining. The test data of non-prestrained samples is shown as black filled circles. The shear moduli of the samples subject to 100 prestraining cycles are all smaller than the mean value of the non-prestrained samples. In the case of $N_{\text{prestrain}} = 50,000$ all values of G_0 are larger than the ones of the non-prestrained samples. However, the stiffness increase after 50,000 prestraining cycles did not exceed 20 % of the stiffness of the non-preloaded specimens although a significant densification was observed ($\varepsilon_v^{\text{acc}}$ up to 6.3 %). Hardly any changes could be detected concerning the curves $G(\gamma)/G_0$ and $D(\gamma)$.

2.3 Cyclic triaxial tests with measurement of P- and S-wave velocity

In cyclic triaxial tests the development of the compression and the shear wave velocity v_p and v_s and the corresponding stiffnesses at small strains E_{s0} and G_0 , respectively with the number of cycles was studied. The test device is shown in Figure 9. The specimen end plates are instrumented with three kinds of piezoelectric elements, i.e. one pair of compression elements (P-wave), one pair of bender elements (S-

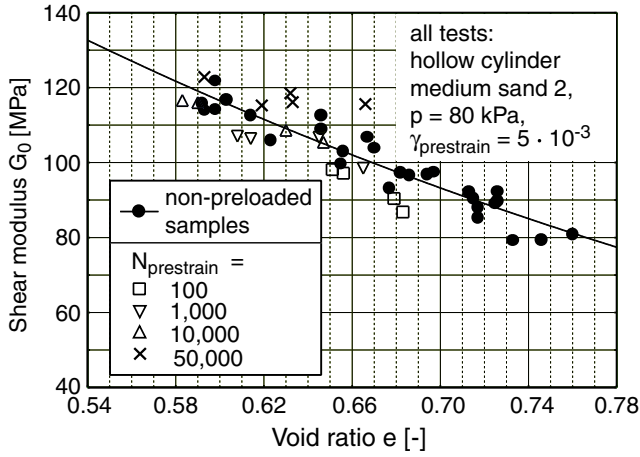


Figure 8. Influence of a cyclic torsional prestraining on small strain shear modulus G_0

Wave) and one pair of shear plates (S-Wave). Wave velocities can be measured in the axial direction of the specimen. Details of the test device can be found in Wichtmann & Triantafyllidis (2004b). The terminology of the cyclic triaxial tests is given by Wichtmann et al. (2004a). An illustration to the tests is presented schematically in Figure 10. After the application of the average stress σ_1^{av} and consolidation (1 h) the wave velocities v_p and v_s were measured. Next the first package with 10 cycles was applied to the specimen. The wave velocities were measured again and then the cyclic loading was continued. In this way v_p and v_s were measured at $\sigma_1^{av} = \text{const.}$ after different numbers of cycles.

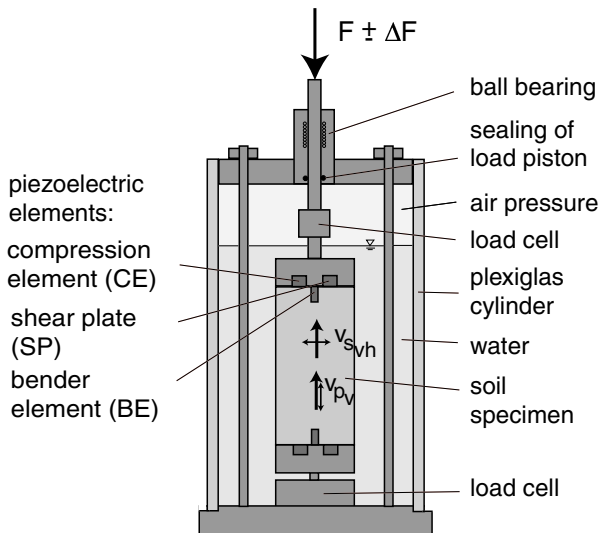


Figure 9. Triaxial device with piezoelectric elements

In the first test series the initial density ($0.59 \leq I_{D0} \leq 0.61$) and the stress amplitude $\sigma_1^{ampl} = 60$ kPa were held constant while the average stress σ_1^{av} was varied ($100 \text{ kPa} \leq p^{av} \leq 200 \text{ kPa}$, $100 \text{ kPa} \leq q^{av} \leq 200 \text{ kPa}$). The dry medium sand 2 was loaded with 100,000 cycles at 1 Hz. Figure 11 shows the development of the small strain stiffnesses E_{s0} and G_0 with the number of cycles. In order to separate the influ-

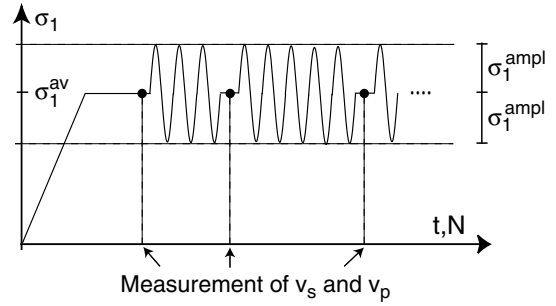


Figure 10. Proceeding of cyclic triaxial tests with measurement of compression and shear wave velocities

ence of fabric changes from the effect of void ratio reduction the stiffnesses were normalized by void ratio functions $F(e)$ (Wichtmann & Triantafyllidis 2004b). Although a significant accumulation of strain $\epsilon^{acc} = \|\epsilon^{acc}\|$ (especially in the case of $p^{av} = q^{av} = 100$ kPa, Fig. 12) was observed only moderate changes of the small strain stiffnesses could be detected. In no test stiffness changes during cyclic loading with 100,000 cycles exceeded 15 % the initial stiffness.

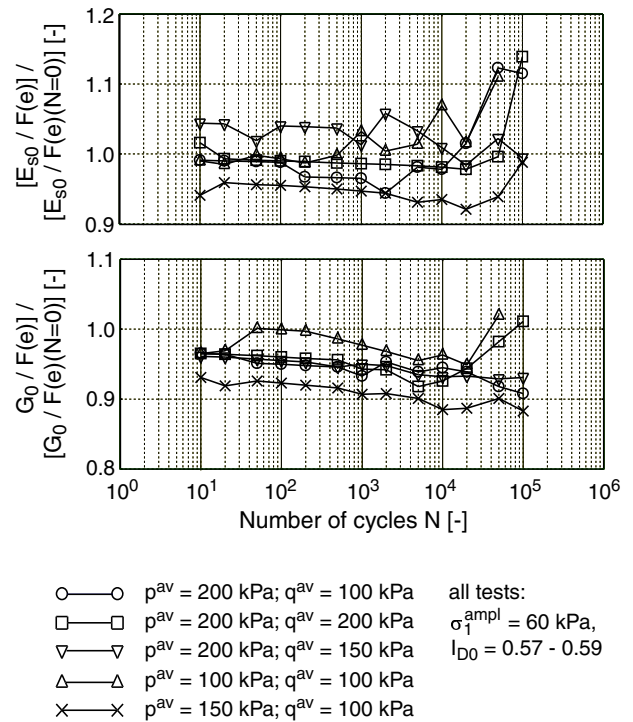


Figure 11. Development of E_{s0} and G_0 with the number of cycles in cyclic triaxial tests with varying average stress σ_1^{av}

Wichtmann & Triantafyllidis (2004b) presented three other test series. In the first series the average and cyclic stresses were held constant ($p^{av} = 200$ kPa, $q^{av} = 150$ kPa, $\sigma_1^{ampl} = 60$ kPa) while the initial density was varied ($0.29 \leq I_{D0} \leq 1.05$). In the second series the average stress ($p^{av} = 200$ kPa, $q^{av} = 150$ kPa) and the initial density ($0.58 \leq I_{D0} \leq 0.61$) were held constant and different stress amplitude ($30 \text{ kPa} \leq \sigma_1^{ampl} \leq 90 \text{ kPa}$) were tested. In a last series of test, additional tests on fine sand were conducted. In neither of

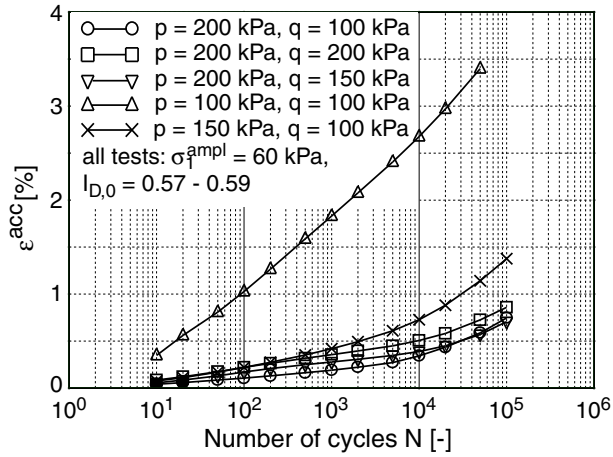


Figure 12. Accumulation of strain ε^{acc} with the number of cycles N in cyclic triaxial tests with varying average stress σ^{av}

these series the stiffness increased after 100,000 cycles more than 10 % of the initial value.

The resonant column tests on cyclically prestrained specimens as well as the cyclic triaxial tests with measurement of compression and shear wave velocities did not show any correlation between cyclic preloading and small strain stiffnesses. Thus, a determination of cyclic preloading history in situ via small strain stiffnesses does not seem to be feasible.

3 CORRELATION OF CYCLIC STRAIN HISTORY WITH MATERIAL DAMPING

In the cyclic triaxial tests documented in subsection 2.3 loss of intensity of the received signals of bender elements and shear plates with the number of cycles was observed while the intensity of the compression element signal stayed almost constant (Wichtmann & Triantafyllidis 2004b). The amplitude of the emitted signal (a single sinus impulse) was not changed during the test. The reduction of the received signal energy with the number of cycles could be caused by an increased material damping. However, a change of the bedding of the elements could also be a possible cause of these observations.

Four additional cyclic triaxial tests were performed on medium sand 2 studying these effects. The experiments concerned bender element measurements as such they produced the clearest signals at the receiver. While the average stress ($p^{\text{av}} = 200$ kPa, $\eta^{\text{av}} = q^{\text{av}}/p^{\text{av}} = 0.75$) was held constant the initial density ($0.59 \leq I_{D0} \leq 0.90$) and the stress amplitude (30 kPa $\leq \sigma_1^{\text{ampl}} \leq 90$ kPa) were varied.

Figure 13 presents the received signals in a test with $\sigma_1^{\text{ampl}} = 60$ kPa and $I_{D0} = 0.59$ after different numbers of cycles N . Although the source signal was a single sinus impulse the received signal contained several crossings of the zero axis due to multiple reflections

at the sample boundaries and probably also due to internal inhomogeneities. The signal intensity grows up to $N = 5,000$ and afterwards a strong abatement was observed. The double amplitude was defined as the span between the total minimum and the total maximum of the signal as demonstrated for $N = 0$ in Figure 13 (keeping in mind, that this measure is influenced by the boundary reflections).

Figure 14 presents the receiver signal amplitude versus N in the four tests. In the tests with small strain accumulation ($\varepsilon^{\text{acc}} \approx 0.1\%$ for $N = 100,000$) only slight changes of signal intensity could be observed due to a high initial density (Test 3) or a low amplitude (Test No. 4). In tests 1 and 2 with higher residual deformation ($\varepsilon^{\text{acc}} \approx 0.8\%$ for $N = 100,000$) an increase of signal intensity up to $N = 2000-5000$ (reduction of material damping?) and a subsequent decrease (increase of material damping or changes of the bender element bedding?) could be detected.

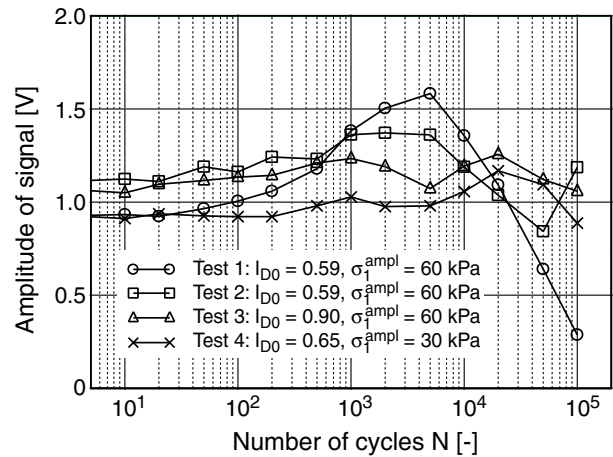


Figure 14. Development of signal amplitude with the number of cycles

The question arises if aging effects (see Afifi et al. 1971, 1973, Baxter 1999, Wichtmann & Triantafyllidis 2004a) could be responsible for the changes in signal intensity. Therefore a test with constant stress $p^{\text{av}} = 200$ kPa, $\eta^{\text{av}} = 0.75$ and an initial density $I_{D0} = 0.70$ was performed without cyclic loading. Over a period of one week the signals were recorded in appropriate time distances but their intensity did not significantly change. Thus, the observations in the cyclic triaxial tests could not be described as aging effects.

In yet another test the receiver signals were acquired over a range of frequencies of the source impulse f_{TRM} (5 kHz $\leq f_{\text{TRM}} \leq 60$ kHz) after every applied package of cycles. Figure 15 shows the received signal amplitude against f_{TRM} for different numbers of cycles. It can be seen that the frequency of the best response, i.e. the location of the peak does not change due to cyclic loading while its height becomes smaller. Evidently there is no shift of the amplitude

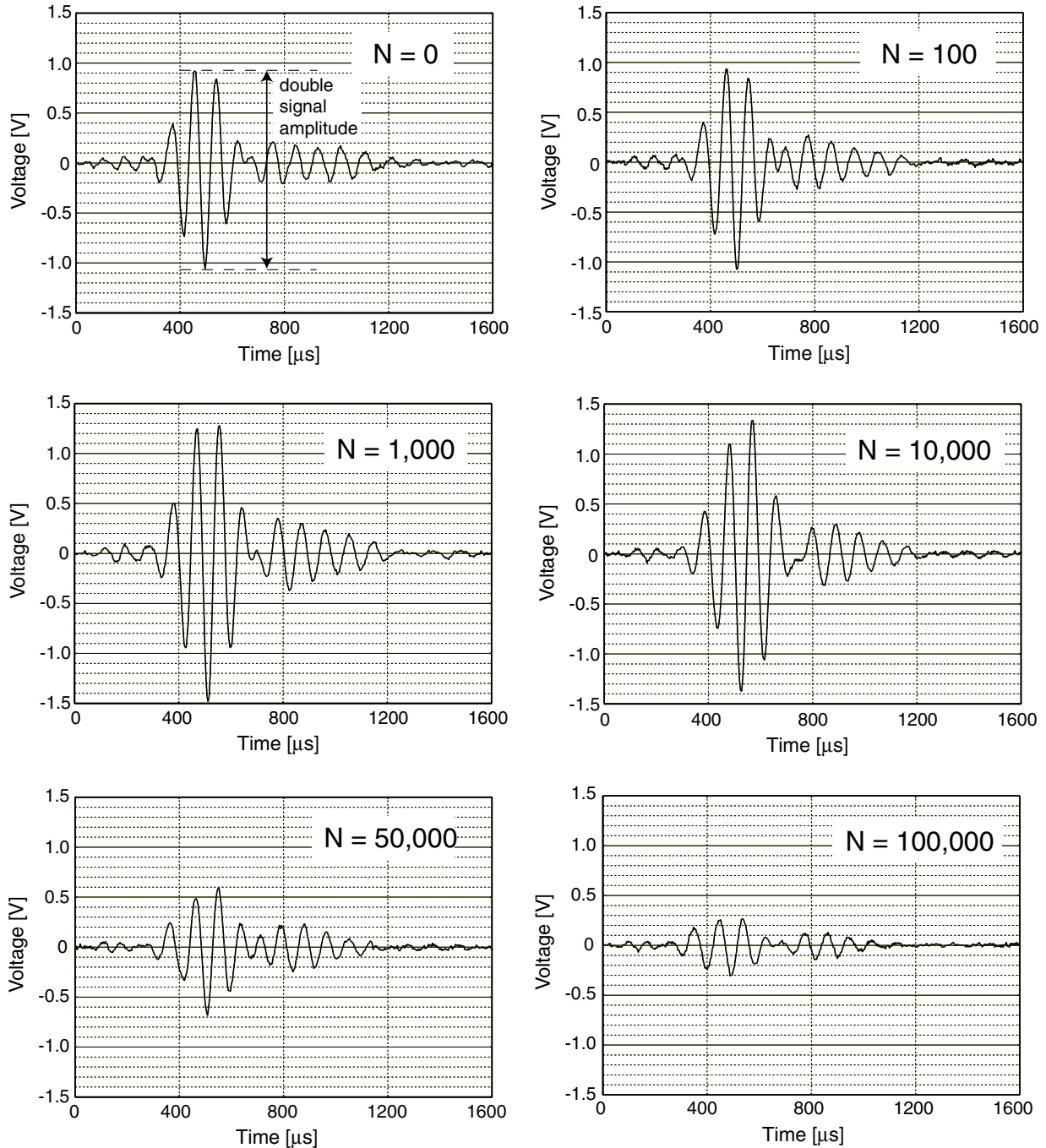


Figure 13. Reduction of the receiver element signal intensity with the number of cycles in a cyclic triaxial test with $p^{av} = 200$ kPa, $q^{av} = 150$ kPa, $\sigma_1^{ampl} = 60$ kPa and $I_{D0} = 0.59$

- frequency spectrum which could explain the abatement of the receiver signals (it is well known that higher frequencies undergo a stronger damping than the lower ones).

The observed effects are somewhat amazing. Resonant column tests on preloaded specimens (cyclic axial preloading in a load press, starting from an isotropic pressure $p^{av} = 80$ kPa applied via vacuum, superimposing $2\sigma_1^{ampl} = 96$ kPa) show a slight but continuous *decrease* of material damping with the number of preloading cycles $N_{prestrain}$ (Fig. 16). Further clarification on this field is necessary.

4 CORRELATION OF CYCLIC PRESTRAINING HISTORY WITH LIQUEFACTION POTENTIAL

4.1 Motivation

The strain accumulation under drained cyclic loading and the pore water pressure increase during cyclic undrained loading are two occurrences of the same phenomenon (just like creep and relaxation). Therefore one could expect that liquefaction is governed by similar structural effects as the accumulation of strain.

Several publications (Finn et al. 1970, Ladd 1974, Mulilis et al. 1975, 1977, Seed et al. 1977, Seed et

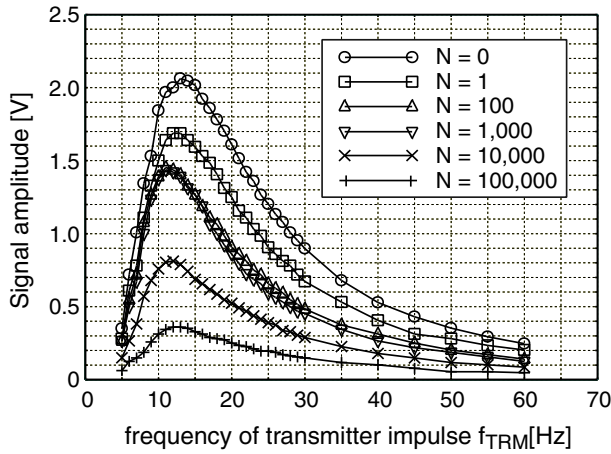


Figure 15. Receiver signal amplitude for varying frequencies of the transmitter signal f_{TRM} after different numbers of cycles N

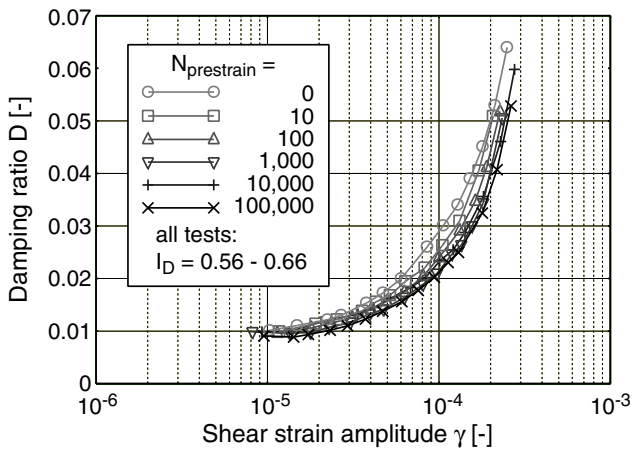


Figure 16. Curves of damping ratio $D(\gamma)$ after different

al. 1988, Teachavorasinskun et al. 1994) documented an impact of cyclic preloading on undrained cyclic strength.

In the study presented in the following cyclic undrained triaxial tests were performed (see also Poblete 2004).

4.2 Cyclic undrained tests without drained preloading

The triaxial device used in the tests was similar to the apparatus presented by of Wichtmann et al. (2004a) with the only difference, that the vertical force was applied by the upper traverse of a free programmable load press driven by an electric servo motor. The actual vertical force was measured by a force transducer inside the pressure cell below the lower end plate. An additional force transducer was mounted below the traverse of the load press. A displacement transducer outside the pressure cell was used to monitor the vertical deformation. Volume changes during consolidation and in the drained test phases were measured by the pore water squeezed out from the sample. Cell pressure and back pressure were monitored by means

of pressure transducers.

The cyclic loads were applied at a constant displacement velocity recording the actual vertical force. This was more convenient than force-controlled testing since the specimen stiffness (which usually varies during a test) affects the control process. Some variations in frequency during the test resulted due to displacement control especially around the initiation of liquefaction. However, the frequencies were generally less than 0.01 Hz and these variations were assumed to be of no importance.

All tests were performed on medium sand 2. The sand specimens were prepared by air-dry pluviation, and saturated first by CO_2 and subsequently by water. A back pressure of 300 kPa was applied. Skempton's B-value was larger than 0.95 in all tests.

In the tests without drained preloading medium dense specimens ($I_D = 0.60-0.65$) were consolidated under isotropic conditions ($p_c = 100$ kPa, $q_c = 0$). Then the specimen drainage was closed and the vertical total stress σ_1 was cyclically varied by σ_1^{ampl} while the lateral total stress σ_3 was kept constant.

Figure 17 presents the increase of pore pressure u and the accompanying decrease of the effective vertical and lateral stresses σ_1' and σ_3' during undrained cyclic loading in a typical test. If the pore water pressure reached the total lateral stress σ_3 the specimen had undergone "initial liquefaction" (here after approximately 1,700 seconds) followed by the well known cyclic mobility phenomenon (e.g. Seed & Lee 1966).

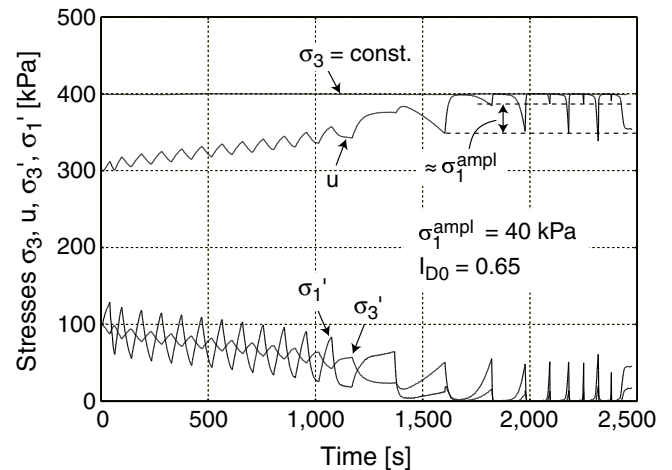


Figure 17. Development of pore water pressure and effective lateral and vertical stresses during undrained cyclic loading

While the vertical strain amplitude $\varepsilon_1^{\text{ampl}}$ was very small during the first cycles it increased strongly during the cycle that lead to initial liquefaction (Fig. 18) and grew with each subsequent cycle. The generated strain amplitudes were nearly symmetric in extension and compression. Figure 19 presents the stress-strain hysteresis and the stress path is shown in Figure 20.

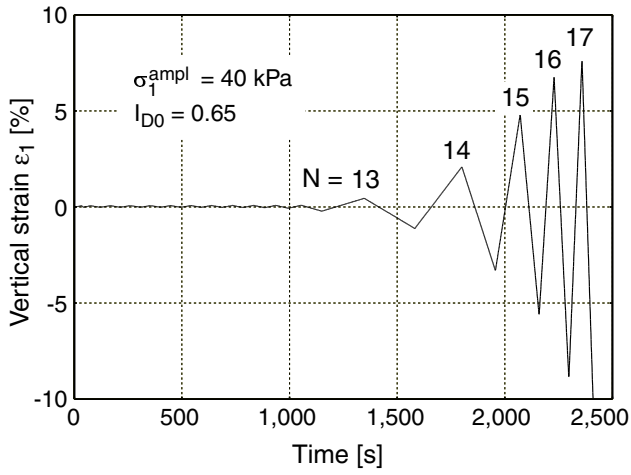


Figure 18. Development of axial strain during undrained cyclic loading

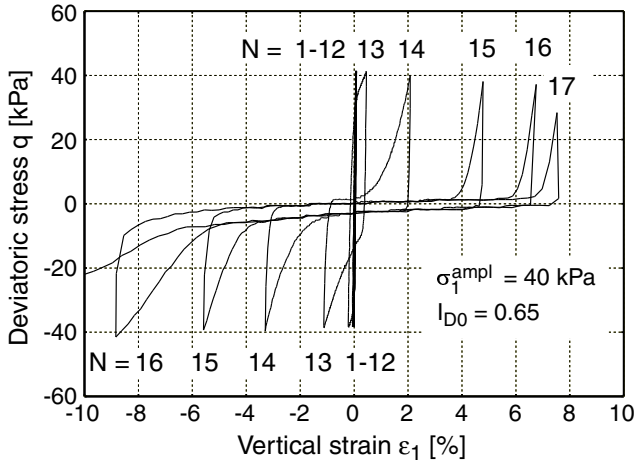


Figure 19. Stress-strain hysteresis for different numbers of cycles during undrained cyclic loading

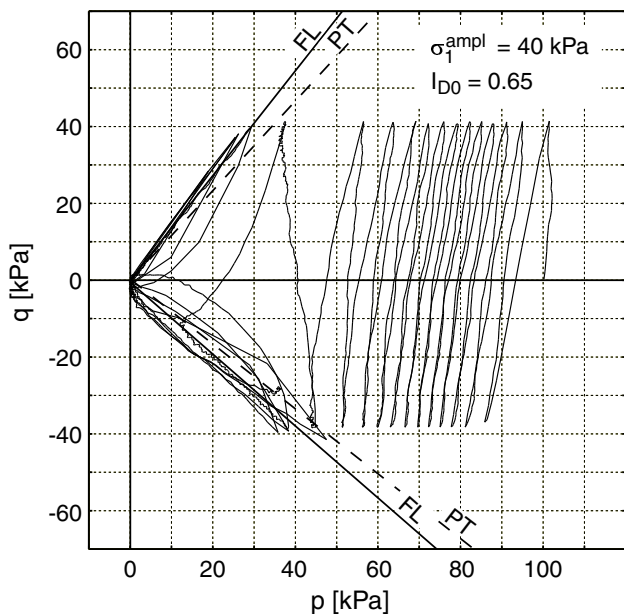


Figure 20. Stress path in the p - q -plane, PT: phase transformation line, FL: failure line (from static tests)

Seven tests with identical consolidation stress ($p_c = 100$ kPa, $q_c = 0$), similar densities ($0.60 \leq I_{D0} \leq 0.65$) but different stress amplitudes σ_1^{ampl} were performed. Figure 21 presents the stress ratios $\sigma_1^{\text{ampl}}/p_c$ and the corresponding cycle numbers that were necessary to generate 2, 5 or 10 % double amplitude vertical strain $2\varepsilon_1^{\text{ampl}}$. The sample was defined as fully liquefied at $2\varepsilon_1^{\text{ampl}} = 10\%$. It is obvious that higher stress amplitudes caused earlier liquefaction. Only a short time was needed between the initial and full liquefaction.

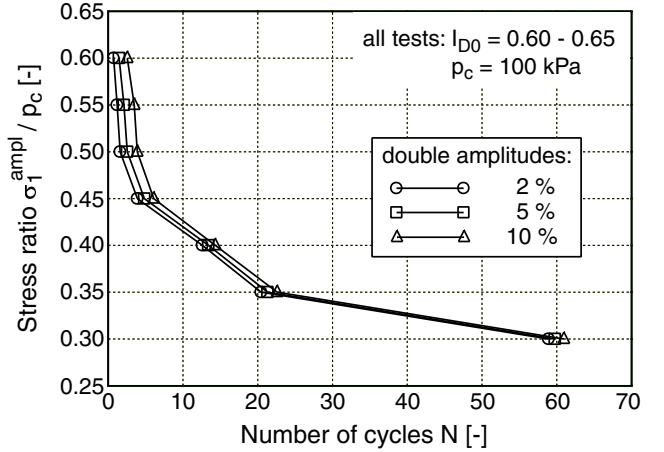


Figure 21. Relationship between stress ratio $\sigma_1^{\text{ampl}}/p_c$ and the number of cycles to cause 2,5 or 10 % double amplitude of vertical strain

5 Cyclic undrained tests with drained preloading

The impact of drained cyclic preloading on the undrained cyclic behaviour was studied in several triaxial tests. All specimens were prepared with densities in the range $0.63 \leq I_{D0} \leq 0.68$ and isotropically consolidated under $p_c = 100$ kPa. Thereafter, a drained cyclic preloading with $\sigma_{1,\text{preload}}^{\text{ampl}}$ and N_{preload} was applied (stress-controlled). The accumulation of strain was measured. After preloading the drainage was closed and the undrained cyclic phase was started.

Three different preloading histories were tried out, Table 2. The stress amplitudes $\sigma_1^{\text{ampl}} = 30$ kPa and $\sigma_1^{\text{ampl}} = 50$ kPa lead to shear strain amplitudes of approximately $\gamma^{\text{ampl}} = 3.3 \cdot 10^{-4}$ and $\gamma^{\text{ampl}} = 7.2 \cdot 10^{-4}$, respectively during preloading. Several amplitudes σ_1^{ampl} during the undrained phase were applied for each preloading history in order to evaluate curves $\sigma_1^{\text{ampl}}/p_c(N)$ analogously to those in Figure 21.

Some of the volumetric accumulation curves are shown in Figure 22. For each preloading history three curves $\varepsilon_v^{\text{acc}}(N)$ are presented. As could be expected the cyclic preloading with an amplitude of 30 kPa causes less accumulation than with 50 kPa. The deviatoric accumulation $\varepsilon_q^{\text{acc}}$ was negligible since the average state of stress was isotropic.

Preloading history	$\sigma_{1,\text{preload}}^{\text{ampl}}$ [kPa]	N_{preload} [-]
1	30	10
2	50	10
3	50	100

Table 2. Tested preloading histories

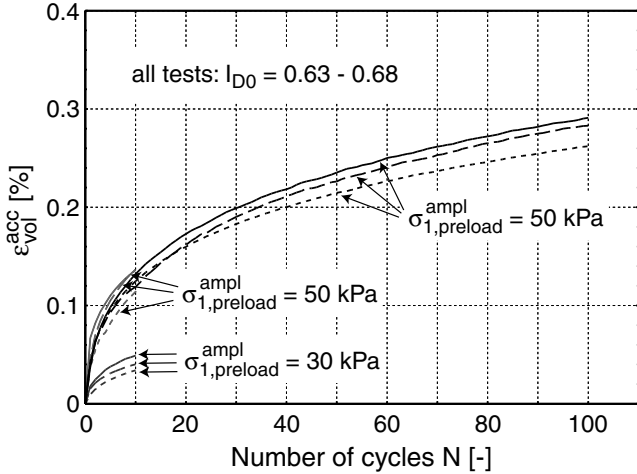


Figure 22. Volumetric strain accumulation curves due to drained cyclic preloading with different stress amplitudes

The development of the pore pressure in four tests with different preloading histories but identical amplitude $\sigma_1^{\text{ampl}} = 45$ kPa in the undrained phase can be found in Figure 23. An increase of the intensity of drained cyclic preloading (in the amplitude and/or in the number of cycles) reduces the rate of pore pressure accumulation $\dot{u} = \partial u / \partial N$ and it takes more cycles to reach initial and full liquefaction. The non-preloaded specimens needed about 5 cycles to initial liquefaction whereas 8 cycles were necessary in the case of the specimen preloaded with $\sigma_{1,\text{preload}}^{\text{ampl}} = 30$ kPa and $N_{\text{preload}} = 10$. The preloading with $\sigma_{1,\text{preload}}^{\text{ampl}} = 50$ kPa and $N_{\text{preload}} = 10$ caused the initial of liquefaction to occur after 43 cycles and 205 cycles were needed for the specimen preloaded with $\sigma_{1,\text{preload}}^{\text{ampl}} = 50$ kPa and $N_{\text{preload}} = 100$. The stress ratios $\sigma_1^{\text{ampl}}/p_c$ and the number of cycles necessary to cause 10 % double amplitude of vertical strain $2\varepsilon_1^{\text{ampl}}$ are shown in Figure 24. It is therefore obvious that preloading may considerably delay liquefaction.

The undrained cyclic strength is defined here as the stress ratio $\sigma_1^{\text{ampl}}/p_c$ necessary to cause 10 % double amplitude vertical strain in 25 cycles. Non-preloaded specimens exhibited an undrained cyclic strength of about 0.35. Preloading with $\sigma_{1,\text{preload}}^{\text{ampl}} = 30$ kPa and $N_{\text{preload}} = 10$ increased the undrained cyclic strength to 0.39, preloading with $\sigma_{1,\text{preload}}^{\text{ampl}} = 50$ kPa and $N_{\text{preload}} = 10$ lead to 0.48 and a preloading with $\sigma_{1,\text{preload}}^{\text{ampl}} = 50$ kPa and $N_{\text{preload}} = 100$ caused the undrained

cyclic strength to increase to 0.55. If the amplitudes in the undrained phase were much higher than the preloading amplitudes the curves $\sigma_1^{\text{ampl}}/p_c(N)$ of the preloaded specimens fell together with the curves of the non-preloaded ones, i.e. cyclic preloading does not affect subsequent pore pressure accumulation induced by substantial larger cycles.

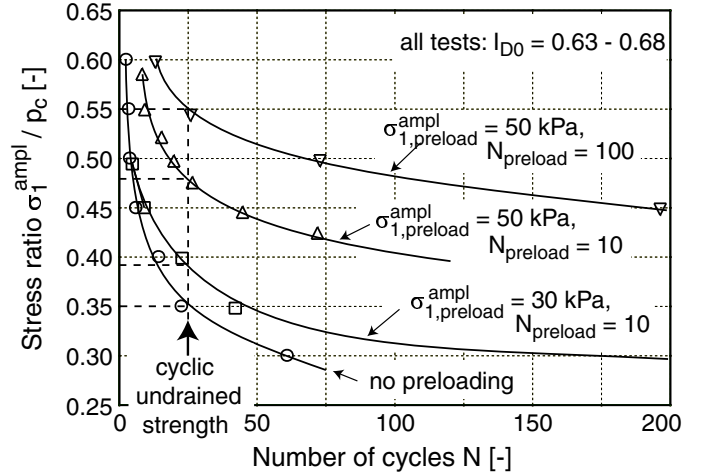


Figure 24. Relationship between the stress ratio $\sigma_1^{\text{ampl}}/p_c$ and the number of cycles to cause 2,5 or 10 % double amplitude of vertical strain for varying preloading histories

It was demonstrated that a drained preloading significantly decreases the rate of pore water pressure rise under undrained conditions and thus, increases the cyclic undrained strength of a soil. A clear correlation between the intensity of the cyclic preloading and the undrained cyclic behaviour exists. Next the transfer of this result on the *in situ* determination of preloading history (e.g. via cone penetration tests with measurement of pore water pressure rates) has to be considered. Note that this method is restricted to fully saturated soils. For partly saturated deposits the situation is more complex.

6 BACK ANALYSIS

As an alternative way to assess cyclic preloading history (at least for soil layers near the surface) one may consider the application of a cyclic test *in situ* using heavy vibration on the soil surface (Fig. 25). The settlement as a function of time or cycles $s(t)$ or $s(N)$ can be recorded. The corresponding boundary value problem can be computed (Niemunis et al. 2004) and the constitutive parameters discussed by Wichtmann et al. (2004a,b) can be used (measured from disturbed samples). The only problem left is the determination of the preloading parameter (accumulated structural strain $\varepsilon^{\text{acc } A}$, see Wichtmann et al. 2004 and Niemunis et al. 2004). This can be done by varying $\varepsilon^{\text{acc } A}$ until the curve $s(N)$ obtained from the heavy vibration is reproduced. Having the preloading parameter

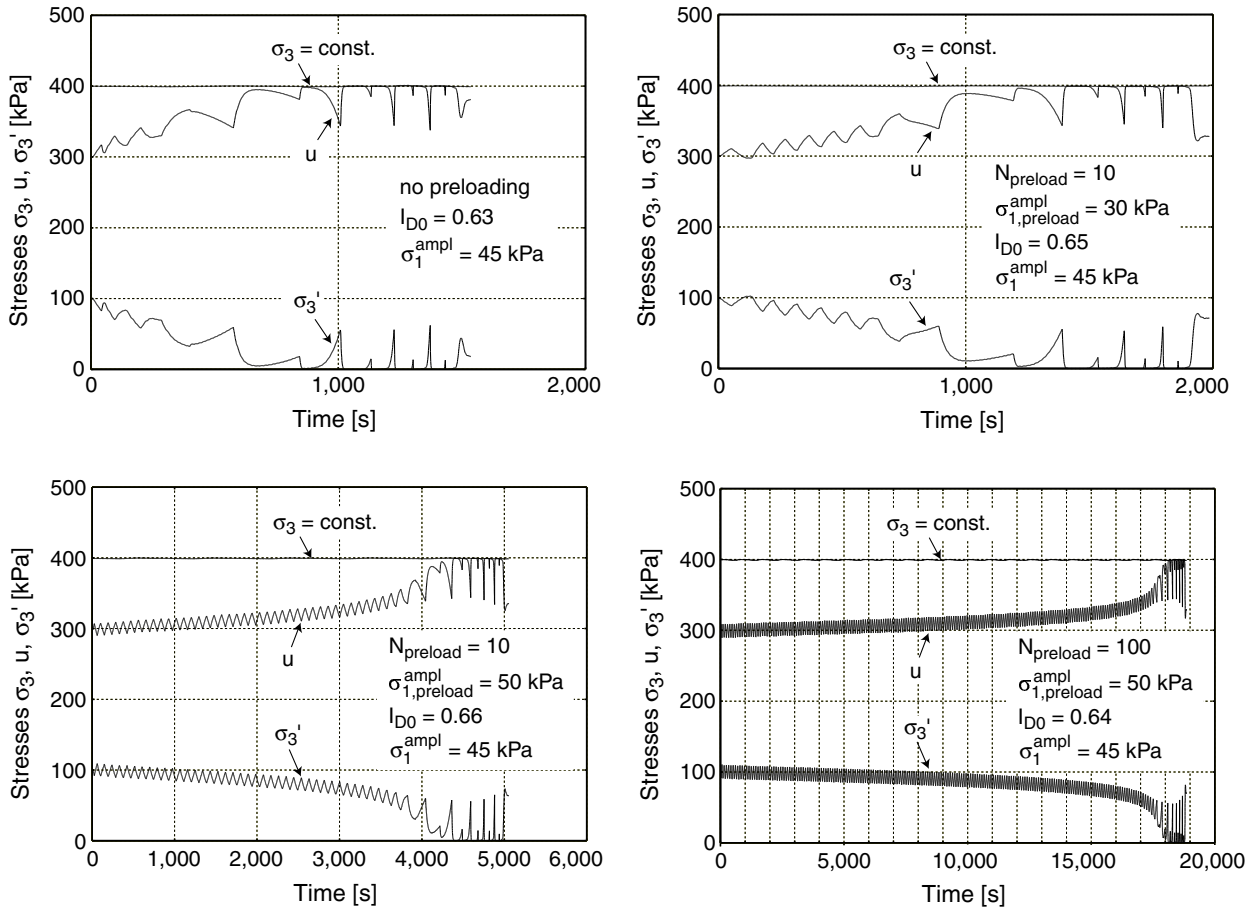


Figure 23. Development of pore water pressure u and effective lateral stress σ_3' during undrained cyclic loading in four tests with varying preloading history (all tests: $\sigma_1^{\text{ampl}} = 45$ kPa in the undrained phase)

from *in-situ* cyclic loading the boundary value problems of interest can be calculated.

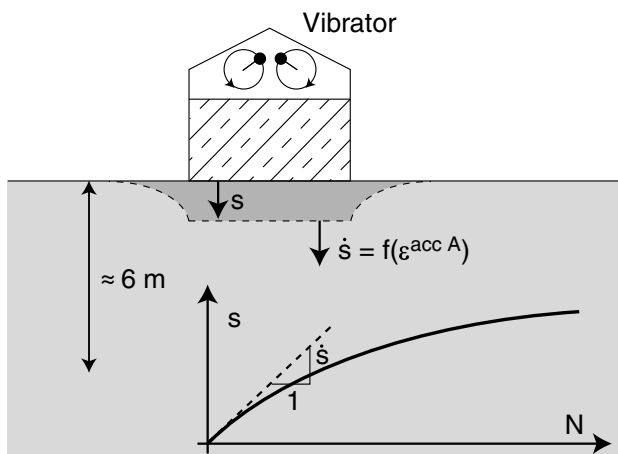


Figure 25. Test loading with a heavy surface vibration *in situ* and back analysis of measured settlement curves $s(t)$

7 SUMMARY AND CONCLUSIONS

Void ratio, average stress and amplitude of cyclic loading are insufficient for the prediction of accumulation rates *in situ*. Cyclic preloading significantly affects the cumulative behaviour and has to be deter-

mined. Several approaches were studied in this paper.

Cyclic preloading could not be correlated with the small strain stiffness. Neither resonant column tests on cyclically preloaded specimens nor cyclic triaxial tests with measurements of compression and shear wave velocities after definite numbers of cycles exhibited significant changes of these stiffnesses due to cyclic loading.

In the cyclic triaxial tests a strong change of the intensity of the received signal was observed. Since resonant column tests show only slight changes (i.e. a moderate decrease) of damping ratio D due to cyclic loading further investigation is necessary.

A cyclic preloading significantly decreases the rate of pore water pressure rise and thus, increases the undrained cyclic strength. A possible conclusion about the preloading *in situ* needs further correlations, e.g. with CPT measurements.

An alternative could be the back analysis of settlement versus time obtained from a heavy vibration *in situ*.

8 ACKNOWLEDGEMENTS

The authors are grateful to DFG (German Research

Council) for the financial support. Parts of the studies presented in this paper were done in the framework of the project A8 "Influence of the fabric changes in soil on the lifetime of structures" of SFB 398 "Life-time oriented design concepts". Other parts were supported by DAAD (German Academic Exchange Program) in the framework of the project "Analytical and Numerical Studies on Microstructure Effects of the Response of Elastic Solids and Structures" as a part of the IKYDA program (Prof. Beskos, Prof. Polyzos, University of Patras). This support is also gratefully appreciated.

REFERENCES

- Afi fi, S.S. & Richart, F.E.Jr. 1973. Stress-history effects on shear modulus of soils. *Soils & Foundations* 13(1): 77-95.
- Afi fi, S.S. & Woods, R.D. 1971. Long-term pressure effects on shear modulus of soils. *Journal of the Soil Mechanics and Foundations Division* 97(SM10): 1445-1460.
- Alarcon-Guzman, A., Chameau, J.L., Leonardos, G.A. & Frost, J.D. 1989. Shear modulus and cyclic undrained behavior of sands. *Soils & Foundations* 29(4): 105-119.
- Baxter, C.D.P. 1999. An experimental study on the aging of sands. PH.D. thesis. Faculty of the Virginia Polytechnic Institute and State University.
- Drnevich, V.P. & Richart, F.E. 1970. Dynamic prestraining of dry sand. *Journal of the Soil Mechanics and Foundations Division* 96(SM2): 453-467.
- Finn, W.D.L., Pickering, D.J. & Bransby, P.L. 1970. Effect of strain history on liquefaction of sand. *Journal of the Soil Mechanics and Foundations Division* 96(SM6): 1917-1934.
- Goddard, J.D. 1990. Nonlinear elasticity and pressure-dependent wave speeds in granular media. *Proceedings of the Royal Society London* 430: 105-131.
- Hertz, H. 1881. Über die Berührung fester elastischer Körper. *Journal reine und angewandte Mathematik* 92: 156-171.
- Ladd, R.S. 1974. Specimen preparation and liquefaction of sands. *Journal of the Geotechnical Engineering Division* 100(GT10): 1180-1184.
- Li, X.S. & Yang, W.L. 1998. Effects of vibration history on modulus and damping of dry sand. *Journal of Geotechnical and Geoenvironmental Engineering* 124(11): 1071-1081.
- Li, X.S., Yang, W.L., Chen, C.K. & Wang, W.C. 1998. Energy-injecting virtual mass resonant column system. *Journal of Geotechnical and Geoenvironmental Engineering* 124(5): 428-438.
- Li, X.S. & Cai, Z.Y. 1990. Effects of low-number previbration cycles on dynamic properties of dry sand. *Journal of Geotechnical and Geoenvironmental Engineering* 125(11): 979-987.
- Lo Presti, D.C.F., Pallara, O., Lancellotta, R., Armandi, M. & Maniscalco, R. 1993. Monotonic and cyclic loading behaviour of two sands at small strains. *Geotechnical Testing Journal* (4): 409-424.
- Mulilis, J.P., Seed, H.B., Chan, C.K., Mitchell, J.K. & Arulanandan, K. 1977. Effects of sample preparation on sand liquefaction. *Journal of the Geotechnical Engineering Division* 103(GT2): 91-108.
- Niemunis, A., Wichtmann, T. & Triantafyllidis, Th. 2004. Explicit accumulation model for cyclic loading. In *International Conference on Cyclic Behaviour of Soils and Liquefaction Phenomena, Bochum, 31 March - 02 April*. Balkema.
- Poblete, M. 2004. Estimation of the cyclic preloading history of a soil by means of liquefaction potential (in German / Spanish). Diploma thesis, Institute of Soil Mechanics and Foundation Engineering, Ruhr-University Bochum.
- Seed, R.B., Lee, S.R. & Jong, H.-L. 1998. Penetration and liquefaction resistances: Prior seismic history effects. *Journal of Geotechnical Engineering* 114(6): 691-697.
- Seed, H.B. & Lee, K.L. 1966. Liquefaction of saturated sands during cyclic loading. *Journal of the Soil Mechanics and Foundations Division* 92(SM6): 105-134.
- Seed, H.B., Mori, K. & Chan, C.K. 1977. Influence of seismic history on liquefaction of sands. *Journal of the Geotechnical Engineering Division* 103(GT4): 257-270.
- Shen, C.K., Li, X.S. & Gu, Y.Z. 1985. Microcomputer based free torsional vibration test. *Journal of Geotechnical Engineering* 111(8): 971-986.
- Teachavoransinskun, S., Tatsuoka, F. & Lo Presti, D.C.F. 1994. Effects of cyclic prestraining on dilatancy characteristics and liquefaction of sand. In Shibuya, Mitachi & Miura (eds): *Pre-failure deformation of geomaterials*: 75-80
- Triantafyllidis, Th. & Niemunis, A. 2000. Offene Fragen zur Modellierung des zyklischen Verhaltens von nichtbindigen Böden. In *Beiträge zum Workshop: Boden unter fast zyklischer Belastung: Erfahrungen und Forschungsergebnisse, Bochum*, Report No. 32: 109-134
- Wichtmann, T., Sonntag, T. & Triantafyllidis, Th. 2001. Über das Erinnerungsverhalten von Sand unter zyklischer Belastung. *Bautechnik* 78(12): 852-865.
- Wichtmann, T. & Triantafyllidis, Th. 2004a. Influence of a cyclic and dynamic loading history on dynamic properties of dry sand, part I: cyclic and dynamic torsional prestraining. *Soil Dynamics and Earthquake Engineering* (accepted).
- Wichtmann, T. & Triantafyllidis, Th. 2004b. Influence of a cyclic and dynamic loading history on dynamic properties of dry sand, part II: cyclic axial preloading. *Soil Dynamics and Earthquake Engineering* (accepted).
- Wichtmann, T., Niemunis, A. & Triantafyllidis, Th. 2004a. Strain accumulation in sand due to drained uniaxial cyclic loading. In *International Conference on Cyclic Behaviour of Soils and Liquefaction Phenomena, Bochum, 31 March - 02 April*. Balkema.
- Wichtmann, T., Niemunis, A. & Triantafyllidis, Th. 2004b. The effect of volumetric and out-of-phase cyclic loading on strain accumulation. In *International Conference on Cyclic Behaviour of Soils and Liquefaction Phenomena, Bochum, 31 March - 02 April*. Balkema.